INSTITUTE FOR FUSION STUDIES

DOE/ET-53088-581 IFSR #581

Linked Mirror Neutron Source

V.P. PASTUKHOV[a] and H.L. BERK
Institute for Fusion Studies
The University of Texas at Austin
Austin, Texas 78712

November 1992

[a] *I.V. Kurchatov Institute of Atomic Energy, 123182 Moscow, Russia*

THE UNIVERSITY OF TEXAS

AUSTIN

Linked Mirror Neutron Source

V.P. Pastukhov[a)] and H.L. Berk
Institute for Fusion Studies
The University of Texas at Austin
Austin, Texas 78712

Abstract

A toroidally linked mirror system is proposed as a neutron source. The mirror core has the favorable feature of a high plasma beta in a relatively small volume. A low beta highly elliptical toroidal linkage prevents rapid electron thermal loss and enhances the power efficiency from $\sim$ 2%, typical for previous designs, to 30%-40%. The following specific problems are discussed: low-β toroidal MHD equilibrium, finite-β distortion of the plasma column, radial electric field, particle drift orbits, rotational stability, beam ion kinetics, cross-field transport.

[a)]Permanent address: I.V. Kurchatov Institute of Atomic Energy, 123182 Moscow, Russia

I. Introduction

Previous studies of a mirror-based beam-target neutron source[1-3] have emphasized that the proven high β (β is ratio of plasma pressure to magnetic field pressure) containment inherent in mirror systems is highly advantageous for testing materials in a fusion environment. Particularly, these systems satisfy the following basic requirements of a "good" neutron source [4]:

1. Relative simplicity and low cost (both capital and operational).

2. Providing the desired fluence in reasonable time.

3. Providing the same 14 MeV secondary neutron spectrum as that of a fusion reactor.

Generally, due to rapid electron thermal loss along magnetic field lines, the electron temperature, T_e, is low in open-ended beam-target systems. This condition limits the hot (beam) ion energy lifetime and correspondingly the source power efficiency both of which are proportional to $T_e^{3/2}$. If T_e can be improved, a major upgrade in efficiency arises.

To prevent the rapid thermal end loss, toroidal mirror devices have been proposed in the past.[5] Here we consider a variant of this idea where we consider a low-β toroidal linkage of the target plasma where the cross-section of the linkage is elliptically shaped. We estimate that such a linkage allows an enhancement of T_e of up to 2 keV in comparison with $0.2 - 0.4$ keV discussed in the previous mirror-based beam-target neutron source proposals,[2,3] which in turn improves the power efficiency Q from $\sim$ 2% to 30%-40%. The enhanced efficiency also allows more flexibility and reliability of the neutron source with respect to different materials test regimes. For example, it allows for a given injection power of $P_{\rm inj} \sim 50$ MW, an increase in the exposed neutron test surface from 0.2 m^2 to 3 m^2, as well as a wall loading of up 10 MW/m^2. The neutral beam injection power density will be reduced by a factor of

~ 20. In addition it is possible to slightly reduce the plasma density and the magnetic field compared to previous designs.

The advantages achieved in our proposal are primarily through two parameters. The first is that the ratio p_h/p_t is large, typically 10, where p_h is the pressure of the mirror confined hot (beam) ions and p_t is the pressure of the toroidally confined target plasma. The high value of p_h/p_t allows us to sustain a toroidal equilibrium in the simple toroidally linked system without any additional stellarator windings or toroidal current. The second parameter is a high ellipticity ($E \geq 10$) of the plasma cross-section in the toroidal linkage cells. High E-value gives an essential improvement of equilibrium conditions, enhances the toroidal β limit by a factor of ~ 10, reduces neoclassical transport and improves some other technical parameters.

In the following sections we will discuss the key issues of the our proposal: low-β MHD-equilibrium of the toroidally linked beam-target plasma, finite-β distortions of the plasma column, radial electric field, particle drift orbits, rotational stability, cross-field transport, beam ion cooling and scattering, relaxation of warm passing (scattered) ions.

II. Magnetic Configuration and low-β MHD Equilibrium

The magnetic configuration to be discussed is shown in Fig. 1. It consists of four individual or, equivalently, two parallel pairs of minimum-B mirror cells (midplane cross-sections 2, 6, 8, 12) linked by two semitori with cross-sections having high ellipticity (4, 10). The smallness of p_t/p_h allows us to use a purely toroidal magnetic field for the linkage. This field conserves the strong ellipticity ($E \geq 10$) of the mirror end fans (cross-sections 3, 5, 9, 11) along the toroidal cells. The magnetic field in the mirror region is produced by conventional Yin-Yang or baseball coils. The toroidal field is produced by elliptical planar coils. The manufacture of such coils is not a problem for modern technology.[6]

The first problem to be discussed is the plasma equilibrium in a toroidally linked mirror system (TLMS). An anisotropic plasma equilibrium is determined by the following equations:

$$\nabla \cdot \mathbb{P} = \mathbf{j} \times \mathbf{B} \ , \tag{1}$$

$$\nabla \times \mathbf{B} = \mathbf{j} \ , \tag{2}$$

where $\mathbf{j}$ is the plasma current and $\mathbf{B}$ the magnetic field. The pressure tensor is of the form:

$$\mathbb{P} = (p_{\perp h} + p_t)\mathbf{I} + (p_{h\parallel} - p_{h\perp})\mathbf{bb} \ , \tag{3}$$

$\mathbf{b} = \mathbf{B}/B$ and $\mathbf{I}$ is the unit dynamic. The longitudinal component of Eq. (1) is automatically satisfied if $p_{\parallel}$ and $p_{\perp}$ are calculated using a distribution function which depends on the integrals of motion. From the transverse component of Eq. (1) it follows, using standard techniques,[7] that:

$$\mathbf{j}_{\perp} = \left[(p_{\parallel} - p_{\perp})(\mathbf{b} \times \boldsymbol{\kappa}) + \mathbf{b} \times \nabla p_{\perp}\right] / B, \tag{4}$$

$$\boldsymbol{\kappa} = (\mathbf{b} \cdot \nabla) \cdot \mathbf{b} \equiv -\mathbf{b} \times (\nabla \times \mathbf{b}) \ .$$

The longitudinal current $j_{\parallel}$ is found using $\nabla \cdot \mathbf{j} = 0$ and this leads to the relation

$$\frac{\partial}{\partial s}\left[\frac{1}{B^3} j_{\parallel}(B^2 + p_{\perp} - p_{\parallel})\right] = -\mathbf{b} \cdot (\boldsymbol{\kappa} \times \nabla)(p_{\parallel} + p_{\perp})/B^2 \tag{5}$$

with s the distance along a field line. Equation (5) must satisfy the following condition when the field lines are closed:

$$\oint \frac{ds}{B^2} (\mathbf{b} \times \boldsymbol{\kappa}) \cdot \nabla(p_{\parallel} + p_{\perp}) = 0 \ , \tag{6}$$

where the integration is along a field line. Equation (6) is the most important condition of equilibrium. It allows us to find the main characteristics of the pressure distribution across field lines using conventional expansions with respect to low β and paraxiality.

The proposed TLMS exhibits the reflection symmetry relative to plane 1-7 and plane 4-10 (see Fig. 1). Due to this symmetry $j_{\parallel}$ must vanish at the cross-sections 1,4,7,10. Thus

it is sufficient to consider one quarter of the system (between cross-sections 1 and 4). Then Eq. (6) reduces to

$$\int_{s_1}^{s_4} \frac{ds}{B^2} (\mathbf{b} \times \boldsymbol{\kappa}) \cdot \nabla (p_{||} + p_{\perp}) = 0 \, . \tag{6'}$$

We invoke a rather reasonable paraxial approximation to describe a minimum-B system.[7,8] In addition, we assume low-β ($\beta = 2p/B^2 \ll 1$). It can then be shown[7,8] that Eq. (6') implies that the constant $p_{\perp}$ contours in the midplane of a single minimum-B mirror cell have to be concentric circles and $j_{||}$ only has a quadrupole component. In the case of TLMS the toroidal drift will generate a dipole component of $j_{||}$ in the toroidal cell. According to Eq. (6') this current must be closed in the mirror cell. This is achieved if the center of the hot ion pressure distribution shifts from the straight axis of the mirror cell.

To calculate this shift we introduce a coordinate system shown in Fig. 2. In the paraxial approximation a mirror cell magnetic field is to be described by two independent functions $B(z)$, $q(z)$:

$$\begin{aligned} B_z &= B - \frac{x^2}{2}\left(\frac{B''}{2} + q'\right) - \frac{y^2}{2}\left(\frac{B''}{2} - q'\right) \, , \\ B_x &= -x\left(\frac{B'}{2} + q\right) \; ; \qquad B_y = -y\left(\frac{B'}{2} - q\right) \, , \end{aligned} \tag{7}$$

where the prime means d/dz. Following standard procedures,[7,8] we solve the field line equation $dx/B_x = dy/B_y = dz/B_z$ and find that the field line coordinates $x(z)$, $y(z)$ are given by

$$\frac{x(z)}{x_0} = \sqrt{\frac{B_0}{B(z)}} \exp\left\{-\int_0^z \frac{q}{B}\, dz\right\}, \tag{8}$$

$$\frac{y(z)}{y_0} = \sqrt{\frac{B_0}{B(z)}} \exp\left\{\int_0^z \frac{-q}{B}\, dz\right\} \, . \tag{9}$$

The subscript "0" corresponds to the mirror cell midplane ($z = 0$). The curvature and the toroidal cross-section ellipticity take the form:

$$\mathbf{b} \times \boldsymbol{\kappa} \approx \hat{\mathbf{y}} x''(z) - \hat{\mathbf{x}} y''(z) \, , \tag{10}$$

$$E \equiv \frac{y(L)}{x(L)} = \exp\left\{2\int_0^{L/2} \frac{q}{B}\, dz\right\} . \tag{11}$$

The magnetic field will be modeled by the expressions:

$$B(z) = B_0\left[1 + (R-1)\sin^2 \pi\frac{z}{L}\right] , \quad q(z) = q_0 \cos \pi\frac{z}{L} , \frac{-L}{2} < z < \frac{L}{2} , \tag{12}$$

with $R = B_t/B_0$ the mirror ratio.

By assuming a shifted parabolic pressure profile at the mirror midplane we obtain the following pressure distribution:

$$p_h = \widehat{p}_h(z)\left\{1 - \frac{1}{a^2}\left[(x_0 - \Delta_0)^2 + y_0^2\right]\right\} , \quad p_t = \widehat{p}_t\left\{1 - \frac{1}{a^2}\left[(x_0 - \Delta_0)^2 + y_0^2\right]\right\} \tag{13}$$

where $x_0(x,z)$, $y_0(x,z)$ and $\Delta_0(z)$ are to be substituted from Eq. (8), $p_h = p_{h\perp} + p_{h\|}$. The function $\widehat{p}_h(z)$ is to be determined by an angular spread of the hot ions in the velocity space. For estimates, we shall consider $\widehat{p}_h(z) = \widehat{p}_{h0}(1 - 4z^2/\ell_h^2)^{1/2}$ where $\ell_h \ll L$.

In the toroidal region, $\boldsymbol{\kappa} \times \mathbf{b}$ is in the y direction so that the toroidal part of the integral in Eq. (6′) is easily calculated in the lowest order of paraxiality

$$2\int_0^{\pi/2} \frac{d\zeta}{\kappa_t B_t^2} (\mathbf{b} \times \boldsymbol{\kappa}) \cdot \nabla p_t = \pi\, \beta_t \frac{y_0}{a^2}\sqrt{\frac{R}{E}} , \tag{14}$$

where $ds = d\zeta/\kappa_t$ with κ_t the average toroidal cell's curvature and $\beta_t = 2\widehat{p}_t/B_T^2$. In the expression for the mirror part of the integral we assume that the hot plasma is shifted from the magnetic axis by an amount Δ_0. Then from mirror cell symmetry, dimensional analysis and neglecting terms of the order p_t/p_{h0}, one can estimate the expression for the mirror part of the integral:

$$\int_{-L/2}^{L/2} \frac{dz}{|\mathbf{B}|^2} (\mathbf{b} \times \boldsymbol{\kappa}) \cdot \nabla p_h = -\beta_{h0} \frac{y_0 \Delta_0}{a^2 \ell^2}\, \ell_h \tag{15}$$

The effective curvature on the field line where p_h is maximum is Δ_0/ℓ^2, where $\ell \sim L$ (more precisely ℓ depends on magnetic field strength and pressure distribution along field lines, but for the purpose of our estimates we take $R \approx 2$, $E \approx 12$, $\ell_h \ll L$, wherein we find $\ell \sim L/3$).

More precisely ℓ depends on the magnetic field strength and pressure distribution along the field lines which requires detailed calculations for precise evaluation. For $R \approx 2$, $E \approx 12$ and $\ell_h \ll L$ we find $\ell \approx L/3$ which will be the value we shall use for the estimates presented below.

Substituting Eqs. (14) and (15) into Eq. (6′), we obtain

$$\Delta_0 = \frac{\pi}{R\sqrt{RE}} \frac{\ell^2}{\ell_h} \frac{\widehat{p}_t}{\widehat{p}_{h0}} \,. \tag{16}$$

Assuming $\ell_h \approx 4.0a$, $\ell_h = 0.15L$, and that Δ_0 does not exceed ~ 0.2 a, we find the following restriction from Eq. (16):

$$\frac{\widehat{p}_{h0}}{\widehat{p}_t} \gtrsim \frac{\pi}{R\sqrt{RE}} \frac{\ell^2}{\Delta_0 \ell_h} \approx 30 \,. \tag{17}$$

It follows from hot ion kinetic analysis,[9] that the effective hot ion temperature $T_h \approx \varepsilon_b/3$, where $\varepsilon_b \approx 160\,\mathrm{keV}$, is the optimum value of the neutral beam energy. Thus for the desirable value $T_e \approx 2\,\mathrm{keV}$, the inequality (17) will be equivalent to $n_{h0}/n_t \geq 2.5$. This slightly reduces the power efficiency in comparison with the case $n_t \gg n_{h0}$ (see below).

To avoid having a shift Δ_0 and its corresponding restriction on the hot-particle to cold-particle density ratio, it is reasonable to compensate the toroidal cell curvature by slightly bending the mirror cell axis, as shown at Fig. 3. In this case Eq. (6′) takes the following form in the lowest order of paraxiality:

$$-\frac{\pi}{4}\beta_{h0}\ell_h\kappa_m - \beta_{h0}\frac{\Delta_0\ell_h}{\ell^2} + \pi\beta_t\sqrt{\frac{R}{E}} = 0 \tag{18}$$

where κ_m is an effective curvature of the mirror cell axis. Δ_0 vanishes if κ_m is chosen as follows:

$$\kappa_m = \frac{\widehat{p}_t}{\widehat{p}_{h0}} \frac{4}{\ell_h R\sqrt{RE}} \,. \tag{19}$$

For the above parameters and $n_{h0} \approx n_t/2$, Eq. (19) takes the form $\kappa_m \approx 0.4\ L^{-1}$, which demonstrates that the needed mirror cell axis curvature is rather small. To create the above curvature, it suffices to slightly tilt the Yin-Yang coils relative to one another. It is important

to note that the joint effects of mirror ratio R and ellipticity E produce a gain factor of order 10 in Eqs. (16) and (19).

III. Finite-β Distortions of the Plasma Column

There are two kinds of finite-β effects to be expected in the TLMS equilibrium. The first is caused by a dipole $j_{||}$ generated in the toroidal cell and it affects the solution in the lowest order of the paraxial approximation. The dipole $j_{||}$ can significantly distort the plasma equilibrium in the toroidal cell and considerably restrict the toroidal β_t. The second kind of finite-β effect is caused by the quadrupole $j_{||}$ generated mainly in the mirror cell. For conventional mirrors, these effects have been investigated in detail.[7] It was found that quadrupole currents can considerably distort the shape of the plasma cross-section, but they do not prevent β_{h0} from becoming of the order of unity. In the toroidal region it is reasonable to expect that the quadrupole $j_{||}$ influence is considerably less than the dipole $j_{||}$ influence. Therefore, as a first step, we evaluate only dipole $j_{||}$ effects.

First we calculate $j_{||}$ in the toroidal cell using Eq. (5) and the boundary condition $j_{||}|_{\xi=\pi/2} = 0$ (see Fig. 2). To lowest order of β and paraxiality we then find

$$j_{||} = \left(\frac{\pi}{2} - \zeta\right) \frac{4\widehat{p}_t}{B_t a^2} \frac{R}{E} y H \left(1 - \frac{x^2}{a^2} RE - \frac{y^2 R}{a^2 E}\right) , \tag{20}$$

where $H(x)$ is the Heaviside step function. This current generates poloidal magnetic field which perturbs the field line equation and causes a displacement of both field lines and plasma from their zero beta positions. By neglecting toroidicity and writing the perturbed poloidal field as $\widetilde{\mathbf{B}}_\perp = \mathbf{e}_\zeta \times \nabla\psi$, we obtain

$$\Delta_\perp \psi = j_{||} . \tag{21}$$

Equation (21), with $j_{||}$ determined by (20), can be solved analytically in two particular cases, corresponding to either circular or strongly elliptical cross-sections.

In the case of high ellipticity ($E \gg 1$), it is sufficient to consider only the external solution of Eq. (21). Now, taking the parallel current to be in a narrow layer, we find

$$j_{\|} \approx 2B_* \sqrt{\frac{R}{E}} \left(1 - \frac{y^2}{a^2}\frac{R}{E}\right)^{1/2} \frac{y}{a} H\left(1 - \frac{y^2}{a^2}\frac{R}{E}\right) \delta(x) \,, \qquad B_* = 2B_t \beta_t \left(\frac{\pi}{2} - \zeta\right) \Big/ E \,. \quad (22)$$

The solution of Eq. (21) for which $\tilde{\mathbf{B}}(x,y)$ is bounded at infinity, takes the form:

$$\psi = \frac{1}{2\pi} B_* a \sqrt{\frac{E}{R}} \int_{-1}^{1} \xi d\xi \sqrt{1-\xi^2} \ln\left[x^2 + \left(y - \xi\, a\sqrt{E/R}\right)^2\right] \,. \quad (23)$$

$\tilde{B}_x = -\partial\psi/\partial y$ is continuous at $x \to 0$, so that one can write $\tilde{B}_x$ inside the plasma as follows:

$$\tilde{B}_x\Big|_{\text{int}} = \tilde{B}_x\Big|_{\text{ext } x\to 0} = \frac{B_*}{\pi} P\int_{-1}^{1} \frac{\xi d\xi \sqrt{1-\xi^2}}{\left(\xi - \frac{y}{a}\sqrt{\frac{R}{E}}\right)} \,. \quad (24)$$

The expression for $\tilde{B}_y|_{\text{ext}}$ takes the form:

$$\tilde{B}_y\Big|_{\text{ext } x\to 0} = B_* \frac{y}{a}\sqrt{\frac{R}{E}}\sqrt{1 - \frac{y^2}{a^2}\frac{R}{E}}\,\text{Sgn}\, x \,, \quad (25)$$

From Eq. (25) it follows that $\tilde{B}_y|_{\text{ext}}$ is of the order of $\tilde{B}_x$ and has jump at $x = 0$. This means that inside the plasma $\frac{\partial \tilde{B}_y}{\partial x} \approx j_{\|} \gg \left|\frac{\partial \tilde{B}_x}{\partial y}\right|$, where $j_{\|}$ is determined by Eq. (20). Thus, taking into account that $\tilde{B}_y$ is an odd function in x, it is easy to obtain for $\tilde{B}_y$ inside the plasma:

$$\tilde{B}_y\Big|_{\text{int}} = B_* \frac{xy}{a^2} R \,. \quad (26)$$

The mirror cell curvature is much less than the toroidal curvature so that in the mirror cell

$$\frac{\partial}{\partial s}\left(\frac{j_{\|}}{B}\right) \approx 0 \quad (27)$$

everywhere in the mirror cell except in the short hot ion region where $j_{\|}$ drops rapidly to zero. Taking into account Eqs. (27) and (20), one can write $j_{\|}$ in the mirror cell as follows:

$$j_{\|} = 2\pi \frac{B(z)\hat{p}_t}{B_t^2 a^2}\sqrt{\frac{R}{E}}\, y_0 H\left(1 - \frac{x_0^2}{a^2} - \frac{y_0^2}{a^2}\right) \,, \quad (28)$$

where $x_0(x,z)$, $y_0(x,z)$ are determined by Eq. (9).

The mirror cell plasma cross-section varies from being strongly elliptical ($E \gg 1$) to circular. Nevertheless, this variation does not alter estimates of the overall field line displacements. To see this, note that from Eqs. (21) and (28) we obtain for $\tilde{\mathbf{B}}$ near the mirror midplane where the cross-section is circular:

$$\begin{aligned} \tilde{B}_x &= \frac{B_{*0}}{4}\left(1 - \frac{x^2}{2a^2} - 3\frac{y^2}{2a^2}\right) , \\ \tilde{B}_y &= \frac{B_{*0}}{4}\frac{xy}{a^2} \qquad B_{*0} = \pi B_0 \beta_t \sqrt{\frac{R}{E}} . \end{aligned} \tag{29}$$

The field line displacements are determined by the following expressions:

$$\frac{d\Delta_{\beta x}}{dz} = \frac{\tilde{B}_x}{B} ; \qquad \frac{d\Delta_{\beta y}}{dz} = \frac{\tilde{B}_y}{B} . \tag{30}$$

Taking into account Eqs. (24) and (29), we find that the differential displacements (30) along a field line varies by a factor of order of unity. However, for the rough estimates we use, we can ignore this variation and use the high ellipticity expressions (24) and (26).

Field lines are anchored by the hot ions near the mirror midplane, therefore the field line displacements vanish near the mirror midplane, and are a maximum at the center of the toroidal cell ($\zeta = \pi/2$). In accordance with Eq. (30):

$$\Delta_{\beta x}\Big|_{\max} \approx \frac{\pi}{8}\frac{\beta_t}{E}\left(2L + \pi/\kappa_t\right) . \tag{31}$$

Note that the high ellipticity reduces Δ_β by an order of magnitude.

Assuming that the material boundaries limit the maximum displacement to be less than the half width of the elliptical plasma $a/\sqrt{RE}$, we obtain the following toroidal β limit:

$$\beta_t \leq \frac{8}{\pi}\sqrt{\frac{E}{R}}\frac{a}{(2L + \pi/\kappa_t)} \tag{32}$$

which gives a $\beta_t \leq 10\%$ for typical parameters; a rather attractive result. According to Eqs. (24) and (26), $\tilde{\mathbf{B}}$ and correspondingly Δ_β are poloidally nonuniform. As a result finite-β toroidal plasma cross-sections take on bean (or banana) shapes as shown in Fig. 4.

IV. Radial Electric Field Effects

As the system we have described has no rotational transform, the microscopic description of equilibrium implies that the bulk of the particles have orbits which close inside the plasma because of particle drift motion. We need to discuss the particle drift motion in detail.

The only physical way closed drift surfaces arise at low beta is because of poloidal electric fields. This field explicitly drops out from fluid MHD considerations. However, it strongly affects the single particle drift orbits, especially in regard to transport. A qualitative analysis allows one to conclude that due to different drift orbits of passing (toroidally confined) particles compared to trapped (mirror confined) particles, a radial polarization of the plasma column is induced which causes poloidal $\mathbf{E} \times \mathbf{B}$ rotation of the plasma.

To simplify the problem we project the particle drift motion along field lines at the mirror cell midplane. The equilibrium electrostatic potential Φ has to be constant along field lines with an accuracy of up to a logarithm of the longitudinal density variation. Thus the projected $\mathbf{E} \times \mathbf{B}$ drift motion is independent of particle position along a field line. It is reasonable to expect that the Φ = const and the p = const contours are circular at the midplane. Contrary to $\mathbf{E} \times \mathbf{B}$ drift, the field line curvature drift depends on the particle pitch angle and the particle energy. Thus it must be different for different particle species.

Under the above assumptions, the equations of motion of passing ions in terms of midplane coordinates, take the form:

$$\begin{aligned} \frac{dx_0}{dt} &= -y_0 \Omega_\Phi \ , & \frac{dy_0}{dt} &= (x_0 - \Delta_\Phi)\Omega_\Phi - V_{Bi}\sqrt{R/E} \ , \\ \Omega_\Phi &= -\frac{c}{r_0} B_0 \frac{d\Phi}{dr_0} \ ; & V_{Bi} &= \frac{v_\perp^2 + 2v_\parallel^2}{2\omega_{ci}} \kappa_t \ , \end{aligned} \tag{33}$$

where Δ_Φ is a shift of the Φ = const contours from the mirror axis. We have assumed that the projected motion onto the midplane circulates at a uniform rate at a fixed r_0. The electron equations of motion have the same form as Eq. (33), but the curvature drift velocity

V_{Be} is different. It readily follows from Eq. (33) that the drift contours of passing ions and electrons are circles with the centers shifted by

$$\Delta_i = \Delta_\Phi + \frac{V_{Bi}}{\Omega_\Phi}\sqrt{\frac{R}{E}} ,$$
$$\Delta_e = \Delta_\Phi - \frac{V_{Be}}{\Omega_\Phi}\sqrt{\frac{R}{E}} . \tag{34}$$

The equations of motion of the mirror-trapped hot ions take the form:

$$\frac{dx_0}{dt} = -y_0\Omega_\Phi - y_0\Omega_{Bh} , \qquad \frac{dy_0}{dt} = (x_0 - \Delta_\Phi)\Omega_\Phi + x\Omega_{Bh} ,$$
$$\Omega_{Bh} = \frac{(v_\perp^2 + 2v_\parallel^2)}{2\omega_{ch}\ell^2} , \tag{35}$$

where we have used for the curvature in the mirror cell $\boldsymbol{\kappa} = \hat{\mathbf{r}}\, r/\ell^2$, with r a radial coordinate and $\hat{\mathbf{r}}$ is a unit vector. Again the drift contours are circles with shifts of the center given by

$$\Delta_h = \Delta_\Phi\Omega_\Phi/(\Omega_\Phi + \Omega_{Bh}) . \tag{36}$$

When $|\Omega_\Phi| \gg \langle\Omega_{Bh}\rangle$ it is almost obvious that $\langle\Delta_h\rangle$, where $\langle\ldots\rangle$ is velocity space averaging, must be physically identical to the MHD displacement Δ_0 which was discussed above. This assumption follows from the quasineutrality condition on an arbitrary flux tube:

$$\oint \frac{ds}{B}\left(\frac{\partial n_h}{\partial x_0}\langle\Delta_h\rangle + \frac{\partial n_i}{\partial x_0}\langle\Delta_i\rangle - \langle\Delta_e\rangle\frac{\partial n_e}{\partial x_0}\right) = 0 . \tag{37}$$

For $|\Omega_\Phi| \gg \langle\Omega_{Bh}\rangle$, Eq. (37) is readily reduced to

$$\widehat{p}_{h0}\Delta_\Phi\frac{\ell_h}{\ell^2}\left(1 - \frac{\Omega_{Bh}}{\Omega_\Phi}\right) = \frac{\pi\widehat{p}_t}{R\sqrt{RE}} , \tag{38}$$

where in the central cell we have taken $\Delta_i = \Delta_e = \Delta_\Phi$. Combining Eqs. (16), (36), and (38), we find $\langle\Delta_h\rangle = \Delta_0$. Thus an MHD consideration of the equilibrium problem is formally correct when $|\Omega_\Phi| \gg \langle\Omega_{Bh}\rangle$. If the last condition is not satisfied, we can expect an appearance of additional kinetic effects. The minimum potential difference $\delta\Phi$ between the center and edge is determined by just satisfying the inequality, which gives,

$$\left|\frac{e\delta\Phi}{T_e}\right| > \frac{T_h}{2T_e}\frac{a^2}{\ell^2} . \tag{39}$$

An upper allowable limit of $\delta\Phi$ is determined from stability with respect to the rotational mode. To estimate it, we use a standard approach based on an "effective gravity."[10] The $\mathbf{E}\times\mathbf{B}$ drift produces a destabilizing inertial force which is to be described by the following effective gravity $g_\Phi \approx r_0\Omega_\Phi^2$. It must be stabilized by the hot ion component which is acted on by the mirror curvature-driven effective gravity: $g_h \approx -r_0\langle v^2\rangle_h/2\ell^2$. For stability the flux tube averaging of the density weighted total effective gravity must be negative:

$$m_h\, g_h\, n_h \frac{\ell_h}{B_0} + m_i\, g_\Phi\, n_t \left(\frac{\pi}{2}\frac{1}{B_t\kappa_t} + \frac{2L}{B_0(R+1)}\right) < 0\ . \tag{40}$$

Therefore, the upper limit of $\delta\Phi$ takes the form:

$$\frac{e\delta\Phi}{T_e} < \left[\frac{R}{\pi}\frac{\widehat{p}_h}{\widehat{p}_t}\frac{\kappa_t\,\ell_h\,a^4}{\ell^2\rho_{i0}^2}\left(1+\frac{4\kappa_t LR}{\pi(R+1)}\right)^{-1}\right]^{1/2}\ , \tag{41}$$

where $\rho_{i0} = (T_i/m_i)^{1/2}/\omega_{i0}$ is target ion gyroradius at the midplane and we take $T_e = T_i = T$. For typical parameters of the neutron source, the right side of the inequality in Eq. (41) is 5-8. Thus the inequalities (39) and (41) determine a rather wide range of acceptable $\delta\Phi$.

We should also note that the conventional curvature-driven flute mode will be stabilized by hot ions for all reasonable parameters. The equilibrium shift needs to be accounted for in estimating stability. Consider the conventional function U which is the $d\ell/B$ integral weighted by the longitudinal distribution of pressure:

$$U \approx \frac{p_h\,\ell_h}{B_0}\left(1-\frac{r_0^2}{2\ell^2}\right) + \frac{\pi}{2}\frac{p_t}{B_t\,\kappa_t}\left(1+\kappa_t\frac{x_0}{\sqrt{RE}}\right)^2\ . \tag{42}$$

In equilibrium the radial pressure distribution has to be centered at a field line (pressure axis) where the condition $\nabla_\perp U = 0$ is satisfied. This determines the position of the pressure center in the midplane:

$$y_{0c} = 0\ ; \qquad x_{0c} \equiv \Delta_0 = \pi\frac{\widehat{p}_t}{\widehat{p}_{h0}}\frac{\ell^2}{\ell_h\, R\sqrt{RE}}\ . \tag{43}$$

Flute stability corresponds to the negative second derivative of U:

$$\frac{d^2U}{dx_0^2} = -\frac{p_h\,\ell_h}{B_0\,\ell^2} + \pi\frac{p_t}{B_t}\frac{\kappa_t}{RE} < 0\ . \tag{44}$$

Hence we obtain the following stability criterion:

$$\frac{\widehat{p}_h}{\widehat{p}_t} > \pi \frac{\ell^2 \kappa_t}{\ell_h R^2 E} \tag{45}$$

which is readily satisfied.

The next important problem, to be discussed is neoclassical transport. According to Eqs. (34) and (36) the shift of the particle drift trajectories has a term $\widehat{\Delta} \equiv \Delta - \Delta_\Phi$ which depends on particle energy and pitch angle. This term produces nonhomogeneous drift orbits and therefore causes neoclassical transport of particles and energy. The origins of neoclassical transport are well known and have been investigated both for closed[11] and open[7] magnetic confinement systems. However, neoclassical transport in the TLMS has several special features which need specific consideration.

Neoclassical transport of the hot particle is not important because the hot ions slow down too rapidly for significant diffusion to occur. However, the lifetime of the thermal plasma is determined by cross-field transport and we therefore only discuss the neoclassical transport of the target plasma. Contrary to tokamaks and stellarators, neoclassical transport in the TLMS primarily involves the toroidally confined passing particles. The role of the banana width is the quantity $\widehat{\Delta}_{e,i}$, which depends strongly on the electric field. According to Eqs. (34) and (39), the maximum value of $\widehat{\Delta}_{e,i}$ is estimated as

$$|\widehat{\Delta}_{e,i}| \leq 2\kappa_t \ell^2 \frac{T_e}{T_h} \sqrt{\frac{R}{E}} \,. \tag{46}$$

As a rule, electrons and ions exhibit different regimes of drift orbit collisionality. Collisionality of the drift orbits is determined by the value of $\Omega_\Phi \tau$, where τ is the corresponding Coulomb collision time. In the next section the following parameters are found to be appropriate: $n_t = 7.4 \times 10^{20}\,\mathrm{m}^{-3}$, $T_e = 2\,\mathrm{keV}$, $a = 14\,\mathrm{cm}$, $B_0 = 4\,\mathrm{T}$. We obtain from Eqs. (39) and (41) that $0.02 \leq |\Omega_\Phi \tau_e| \leq 0.6$. Thus electron orbits are strongly collisional, and electron

neoclassical thermal conductivity is estimated as follows (see Ref. 7):

$$\chi_e\Big|_{nc} = \frac{(\hat{\Delta}_e \Omega_\Phi \tau_e)^2}{2\tau_e} = \frac{1}{2} V_{Be}^2 \tau_e \frac{R}{E} \,. \tag{47}$$

Note that $\chi_e|_{nc}$ is independent of $\delta\Phi$, but strongly dependent on T_e, scaling as $T_e^{7/2}$. Under the above conditions the ion orbits are in the low collisionality regime $|\Omega_\Phi \tau_i| > 1$. Then we obtain for $\chi|_{nc}$

$$\chi_i\Big|_{nc} \approx \frac{\hat{\Delta}_i^2}{2\tau_i} \approx \frac{\kappa_i^2 a^4}{2RE\tau_i} \left(\frac{T_i}{e\delta\Phi}\right)^2 \,. \tag{48}$$

Thus $\chi_i|_{nc}$ essentially depends on $\delta\Phi$, and its maximum value can exceed $\chi_e|_{nc}$ by as much as $\sqrt{2m_i/m_e}$.

To estimate the self-consistent electric field, we need to discuss cross-field diffusion. It should be noted that diffusion in the TLMS is not automatically ambipolar, because ion-ion and electron-electron collisions cause independent diffusion. There are no restrictions caused by momentum conservation. Therefore, the pitch angle dependence of $\hat{\Delta}_{e,i}$ provides the additional diffusion, with the diffusion coefficient $D_{e,i}$ being comparable to the thermal conductivity coefficient $\chi_{e,i}$. To satisfy the ambipolarity condition, we need to have $D_e = D_i$ and correspondingly $\chi_e \sim \chi_i$. This allows us to estimate Ω_Φ and $\delta\Phi$ from Eqs. (47) and (48):

$$\begin{aligned} |\Omega_\Phi \tau_i| &\approx \left(\frac{2m_i}{m_e}\right)^{1/4} \,, \\ \left|\frac{e\delta\Phi}{T}\right| &\approx \frac{2a^2}{\rho_i^2 \omega_{ci} \tau_i} \left(\frac{2m_i}{m_e}\right)^{1/4} \,. \end{aligned} \tag{49}$$

For the above plasma parameters, Eq. (49) gives $|e\delta\Phi| \approx 3T_e$. This value is within the interval of acceptable $\delta\Phi$, in the inequalities in Eqs. (39) and (41). The resulting $\delta\Phi$ is rather high, and thus the potential well has strong effects on the diffusion and more precise calculations are needed to obtain correct numerical coefficients. However, it is obvious that to achieve ambipolarity, D_i and χ_i will be reduced to values comparable to D_e and χ_e. Therefore, we conclude that both electron and ion neoclassical thermal conductivity must

be of the order of χ_e, which is determined by Eq. (47) and takes on the rather low value of $\chi_e \approx 0.05\,\mathrm{m}^2/\,\mathrm{sec}$ for the above plasma parameters. We would like to emphasize again that high ellipticity E improves plasma confinement as it reduces χ_e, χ_i values.

V. Sustaining a Hot Ion Component and Parameters of the Neutron Source

Sustaining a trapped hot ion component in the good curvature region is the most reliable aspect of our concept because it has been successfully demonstrated experimentally. Its implementation has been discussed in detail, for an open-ended neutron source,[2,3] and for the closed trap Drakon, which is stabilized by an anisotropic pressure anchor.[9] All the appropriate formulas are available in Ref. 9 and here we only present brief remarks and final results.

When $\varepsilon_b/T_e > (m_h/m_e)^{1/3}$ the hot ion distribution function is formed mainly by ion slowing down due to electron drag.[2,3,9] The fast ion drag prevents appreciable pitch angle broadening of the initially injected beam and thereby allows confinement of the hot ion density distribution in the mirror regions. Assuming $\ell_h/L \approx 0.14$ and $R = 2$ and using results of Ref. 9, we have obtained the effective hot ion temperature:

$$T_h \simeq \left\langle \frac{mv_\perp^2}{2} \right\rangle_h \approx \frac{1}{3}\varepsilon_b \tag{50}$$

and a critical ion energy ε_* below which scattering into the loss cone becomes important:

$$\varepsilon_* \equiv \frac{mv_*^2}{2} \approx 10T\,. \tag{51}$$

Using the expressions for the distribution function and for the lifetime of the hot ions,[11] the neutron power efficiency is as follows[1]:

$$Q_N = \frac{P_N}{P_{\mathrm{in}}} = \frac{n_t}{n_t + n_h}\,\frac{G(\varepsilon_b)}{7}\,T_e^{3/2}\,, \tag{52}$$

where P_{in} is the input injected power, P_N the power produced from neutrons, T_e is expressed in keV, and $G(\varepsilon_b)$ has a peak value $G_{\max} = 1$ at $\varepsilon_b = 160\,\mathrm{keV}$.

The hot ion scattering to the loss cone in a closed magnetic trap (contrary to an open trap) produces an additional population of warm passing (scattered) ions. The warm ions might produce some undesirable effects, such as an increased β_t that can induce MHD instability, a limitation of MHD equilibrium, or an enhanced neutron flux in the toroidal cell. The warm ion kinetics have been investigated earlier for Drakon.[12] The results of this investigation allow one to infer the following warm ion temperature T_w and density n_w for the neutron source:

$$T_w \equiv \langle mv^2/3 \rangle_w \approx 2.7\, T_e \ ;$$
$$\frac{n_w}{n_h} = \frac{0.12\, R\ell_h}{(\frac{\pi}{2\kappa_t} + \frac{2R}{R+1} L)} \approx 1.6 \cdot 10^{-2} \ . \tag{53}$$

Thus $\beta_w \ll \beta_t$. The neutron flux produced by warm ions appears to be $\sim 20\%$ of the target plasma neutron flux F_{Nt}. Thus, it appears that the warm plasma component does not cause any significant undesirable effect.

Now we have almost all the relations needed to create a self-consistent model of a linked mirror neutron source. However, two additional issues still need to be addressed. They are the toroidal beta limit with respect to ballooning modes and the determination radial heat transport when drift instability is accounted for. Both issues need further theoretical and experimental investigations. For now, we take the desirable and acceptable values of T_e, B and total injected power $P_{\rm in}$ which ultimately needs to be compatible with constraints imposed by ballooning stability and drift wave transport.

Estimates of the Linked-Mirror Neutron Source parameters are given in Table I. The magnetic system parameters were chosen by taking into account previous minimum-B cell designs[2,4] and assuming that a mirror cell neutron shield thickness must be of the order of 0.6 m. Neutron wall loading and total injected power were chosen approximately the same as in previous neutron source projects.[2,3] However, there is no problem in increasing F_{Nh} up to 10 MW/m^2. Taking into account that there are four separated test cells in TLMS, it is possible to provide different F_{Nh} in the different cells simultaneously. Here the value of $P_{\rm in}$ is

determined by operational cost only, and it could probably be increased up to 100 MW. The D^0 beam energy is 160 keV which is optimal and now available.[1] The ratio $n_t/n_h = 2$ allows β_t to be reduced without causing a considerable reduction of the power efficiency given in Eq. (52). For neutron wall loading estimates we have assumed that radius of the testing wall is $a_w \approx 1.3\,\mathrm{a}$.

Using the results of the previous sections, we have estimated the plasma parameters in TLMS which are presented in Table II.

First, we compare the self-consistent $\beta_t = 0.018$ with the equilibrium beta limit $\beta_t \leq 0.06$ determined by (32). We see that there is a "safety factor" (the ratio of the critical beta value to the self-consistent β value) of ~ 3.

To estimate a cross-field transport "safety factor," it is convenient to introduce a "global" thermal conductivity coefficient χ_{gl} which would allow a desirable target plasma to be sustained for a given P_{in}:

$$\chi_{gl} = \frac{P_{\mathrm{in}}}{16\pi n_t T_e (2L + \pi/\kappa_t)} \,. \tag{54}$$

For the above parameters, we find that $\chi_{gl} \approx 0.3\,\mathrm{m}^2/\,\mathrm{sec}$ which is comparable with experimentally observed values in tokamaks. Formally, we are able to estimate a transport "safety factor" as $\alpha_\chi = \chi_{gl}/2\chi_e|_{nc} \simeq 3$ where $\chi|_{nc}$ is determined by Eq. (47). However, the temperature dependence of α_χ is very strong: $\alpha_\chi \sim T_e^{-9/2}$. Due to this strong dependence, the exact value of α_χ is unimportant. T_e will be fixed near $T_e \approx 2\,\mathrm{keV}$ if anomalous χ is not appreciably more than $\chi_{gl} \approx 0.3 m^2/\,\mathrm{sec}$.

VI. Conclusion

As has been emphasized,[1] the serious development of the fusion program will require extensive materials testing experiments with high intensity neutron sources with neutron energy spectra similar to what would be in a fusion reactor. We think that the linked mirror neutron

source discussed in this paper exhibits all the advantages inherent in a mirror based beam target neutron source.[1] It may provide more than 10 times higher neutron power efficiency than a conventional mirror source and it is still more compact and intense than a tokamak fusion reactor.

We should emphasize that most of the basic physical principles of the source have been proven experimentally; e.g. MHD and kinetic stability, high beta ($\beta \sim 1$), quasi-steady-state operation in the beam-target regime have been demonstrated in 2XIIB[12] and TMX[4] experiments. The experiments[4,13] have also confirmed that classical hot ion slowing down scaling[1,2,9] is produced when the drift cyclotron loss-cone mode is suppressed by the target plasma. Quite significantly, GAMMA-6 experiments[14] have demonstrated a highly elliptical equilibrium ($E \approx 17$) in a long straight cell terminated by two quadrupole hot ion anchors with parallel end fans. This observation is extremely important, as the elliptical toroidal link is essentially the new aspect of our proposal. A careful documentation of elliptically shaped central cells in tandem mirror machines would be extremely useful for this concept.

The hot ion density $n_h \approx 1.5 \cdot 10^{20}\,\mathrm{m}^3$ has also been achieved experimentally.[13] Today, neutral beams with $\varepsilon_b \approx 150\,\mathrm{keV}$ are available at JET[15] with pulse times of 10-20 seconds. The extension to steady-state operation is considered straightforward. Experience in manufacturing large Yin-Yang superconducting coil is also available.[6] The main problems that need to be solved both theoretically and experimentally are the determination of the ballooning β_t limit and whether there is anomalous target plasma cross-field transport as a result of drift wave turbulence. Nevertheless, the above estimates are based on relatively modest assumptions for achieving interesting plasma parameters for a neutron source. More realistic preliminary conceptual designs and intermediate scale experiments are certainly needed to guarantee the reliability of the proposed neutron source.

Acknowledgments

We would like to acknowledge important conversations with V. Ilgisonis. This work was supported by the U.S. Department of Energy contract #DE-FG05-80ET-53088.

References

1. H.L. Berk, D.D. Ryutov, Comments Plasma Phys. Controlled Fusion **13**, 173 (1990).

2. F.N. Coensgen, T.A., Casper, D.I. Correll, C.C. Damm, A.H. Futch, B.G. Logan, A.W. Molvik, and R.H. Bulmer, UCRL 97280, Rev. 1, LLNL (1987).

3. I.A. Kotelnikov, V.V. Mirnov, V.P. Nagornyi, and D.D. Ryutov, Proc. 10^{th} IAEA Conf. on Plasma Phys. and Controlled Nucl. Fusion Res., Vol. 2, (Vienna, 1986) p. 309 (1985).

4. T.C. Simonen (ed.), Summary of Results from Tandem Mirror Experiment (TMX), UCRL 53120, Livermore (1981).

5. J.G. Cordey and C.J. Watson, Proceedings Fusion Reactor Workshop, Culham, 1974, Nucl. Fusion Supplement (Vienna, 1975) p. 199.

6. R.E. Tatro, J.W. Wohlwend, and T.A. Kozman, Proc. 12^{th} Symp. on Fusion Technology, Vol. 1, p. 167, Pergamon Press (1982).

7. D.D. Ryutov and G.V. Stupakov, in *Reviews of Plasma Physics,* Vol. 13, B.B. Kadomtsev (ed.), (Consultants Bureau, New York, 1987).

8. L.D. Pearlstein, T.B. Kaiser, and W.A. Newcomb, Phys. Fluids **24**, 1326 (1981).

9. V.I. Ilgisonis and V.P. Pastukhov, Sov. J. Plasma Phys. **10** (5), 542 (1984).

10. M.N. Rosenbluth and C. Longmire, Ann. of Phys. **1**, 120 (1957).

11. A.A. Galeev and R.Z. Sagdeev, in *Reviews of Plasma Physics*, Vol. 7, M.A. Leontovich (ed.), (Consultants Bureau, New York, 1979).

12. V.I. Ilgisonis, Sov. J. Plasma Phys. **11** (5), 303 (1985).

13. F.H. Coensgen, J.F. Clauser, D.L. Correll, W.F. Cummins, C. Gormezano, B.G. Logan, A.W. Molvik, W.E. Nexsen, T.C. Simonen, B.W. Stallard, and W.C. Turner, Proc. 6^{th} IAEA Conf. on Plasma Phys. and Controlled Nucl. Fusion Res., Vol. 3, p. 135 (1977).

14. S. Miyoshi, K. Sawada, T. Kawabe, K. Yatsu, K. Ishii, A. Itakura, I. Katanuma, H. Ikegami, and S. Hagiwara, Proc. 8^{th} IAEA Conf. on Plasma Phys. and Controlled Nucl. Fusion Res., Vol. 1, p. 113 (1981).

15. H.D. Falter, G.H. Deschamps, R.S. Hemsworth, and P. Massmann, Proc. 15^{th} Symp. on Fusion Technology, Vol. 1, p. 583, North-Holland (1988).

Figure Captions

1. Structure of magnetic field lines in the toroidally linked mirror system. Cross-sections 2, 6, 8, 12 correspond to minimum-B mirror cell midplanes.

2. Coordinate frame. Point $x = y = z = 0$ corresponds to the center of the mirror cell midplane.

3. Plane view of the TLMS with bent mirror cell axis. Cross-sections 2, 3, 8, 12 correspond to mirror cell midplane.

4. Finite-beta distortion of the toroidal cell cross-section. a) low-β; b) finite-β.

Table I: Estimated "Neo-Classical" Parameters of Linked-Mirror Neutron Source

Number of mirror cells	4
Central magnetic field B_0	4 T
Quadrupole field gradient b_0	5 T/m
Toroidal magnetic field B_t	8 T
Mirror cell length L	4 m
Toroidal axis curvature κ_t	0.5 m^{-1}
Maximum neutron wall loading F_{Nh}	7 MW/m^2
Total injected power P_{in}	50 MW
D^0 beam energy ε_b	160 keV
Electron temperature T_e	2 keV
Ratio of hot component length to edge radius ℓ_h/a	4
Target to hot ion density ratio n_t/n_h	2

Table II: Plasma Parameters

Neutron power efficiency Q_N	0.27
Neutron exposed surface S_N	1.9 m^2
Hot component length ℓ_h	0.55 m
Midplane edge radius a	0.14 m
Peak hot ion density	$3.7 \cdot 10^{20}$ m^{-3}
Target plasma density	$7.4 \cdot 10^{20}$ m^{-3}
Peak mirror beta β_h	0.46
Toroidal beta β_t	0.018
Toroidal cell ellipticity E	12
Mirror cell axis curvature κ_m	0.11 m^{-1}
Total toroidal cell neutron flux $F_{Nt} + F_{Nw}$	1.7 kW/m^2

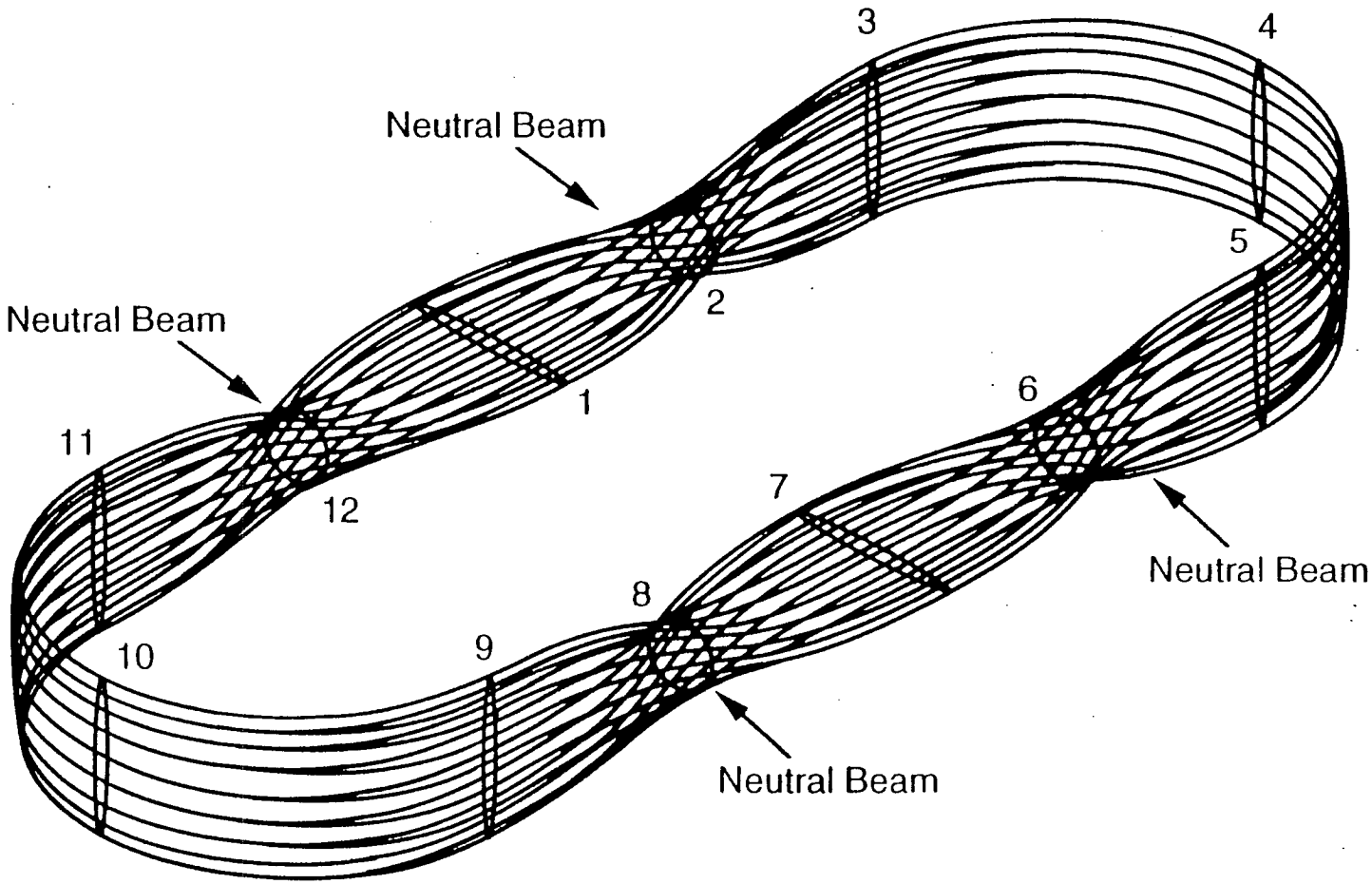
3
4
Neutral Beam
5
2
Neutral Beam
1
6
11
7
12
Neutral Beam
8
10
9
Neutral Beam

Figure 1

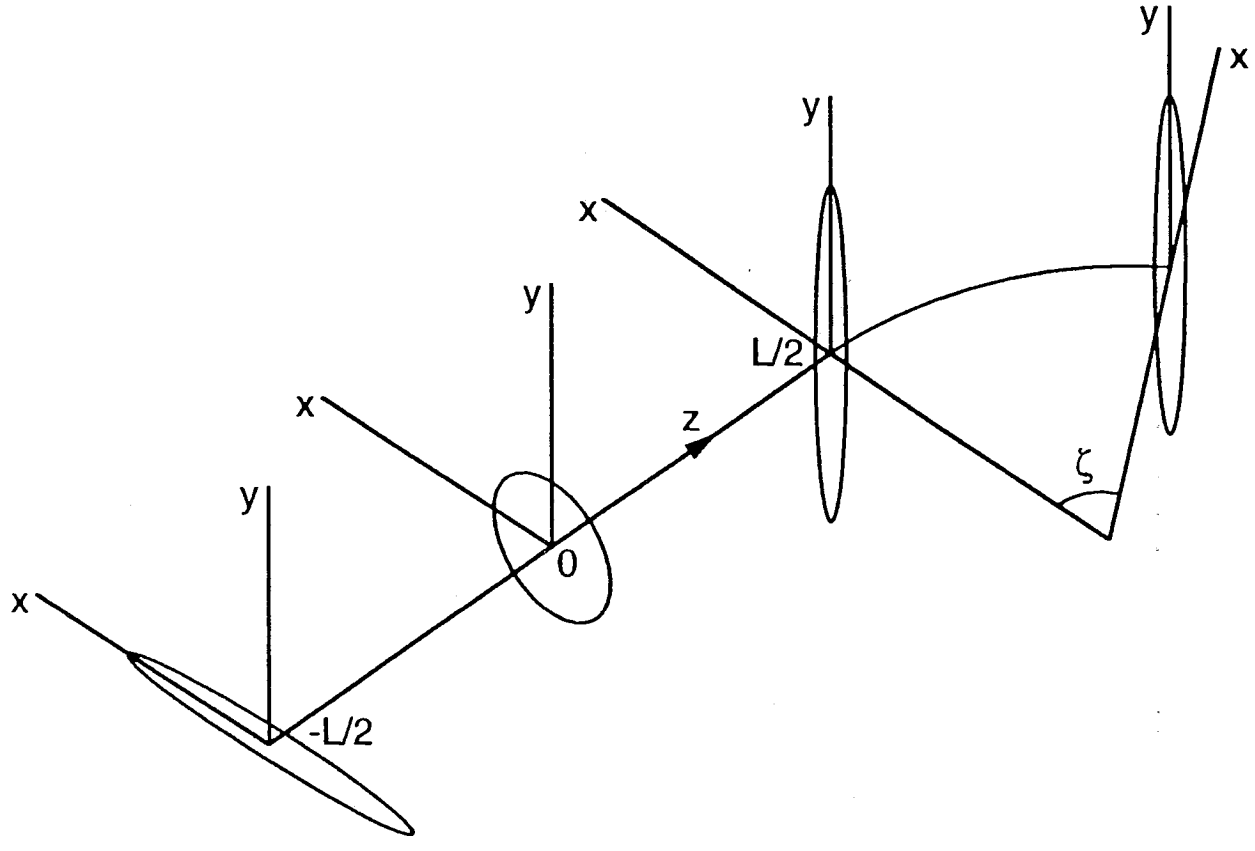

Figure 2

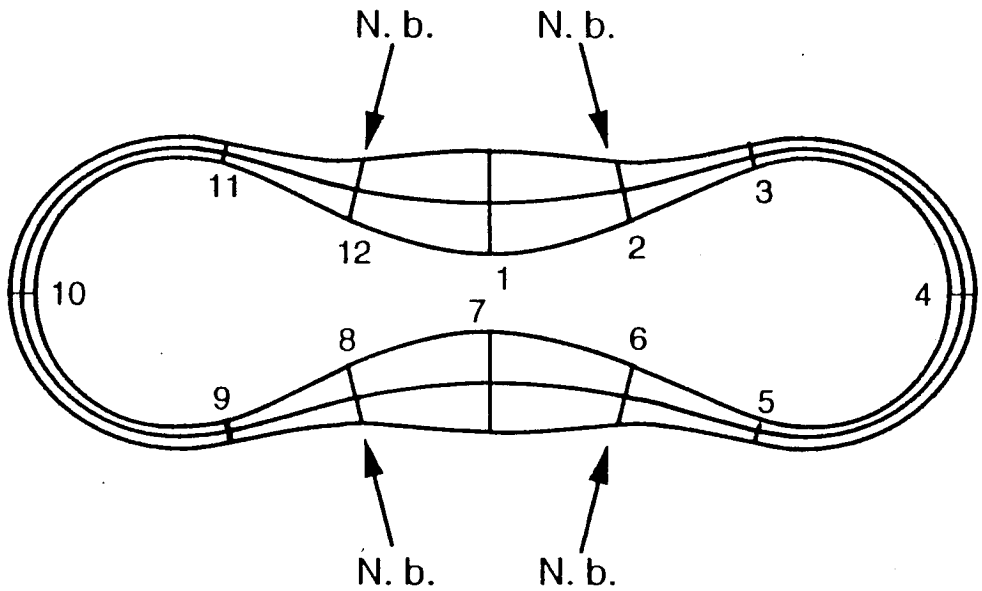

Figure 3

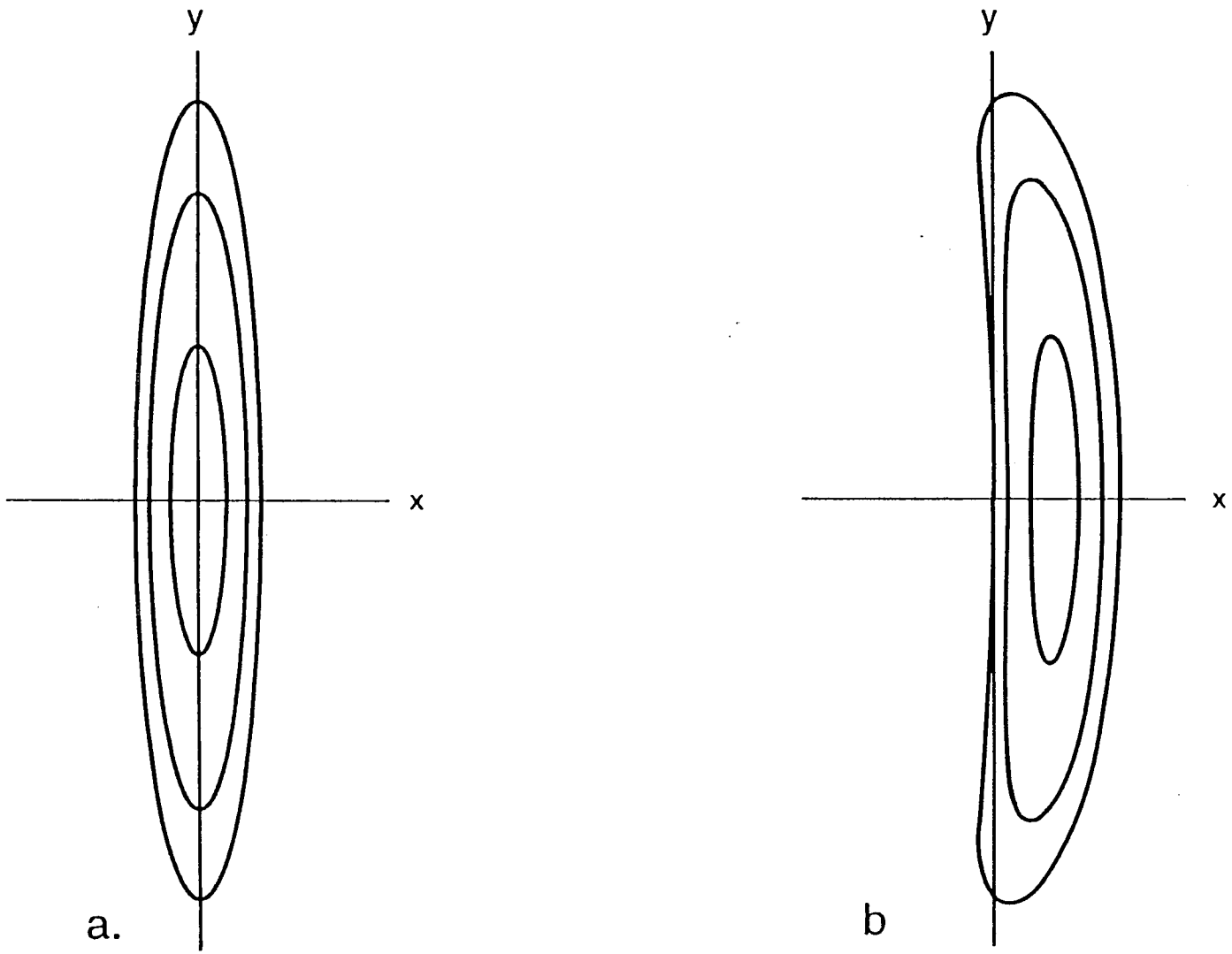

Figure 4